SOFT ROBOTICS
Volume 00, Number 00, 2026

DOI: 10.1177/21695172251400152

SoRo
Soft Robotics

ORIGINAL ARTICLE

High-Degree-of-Freedom Fabric-Based Soft Glove with Dexterous Thumb Assistance Assistance

Jianing Sun, Miao Feng, Dezhi Yang, Yexun Wei, and Guoying Gu

Abstract

Fabric-based soft gloves, due to their safety, light weight, and compliance, exhibit promising potential in assisting individuals with hand impairments. However, most existing soft gloves focus solely on finger flexion and extension, with limited consideration for thumb assistance. This restricts their effectiveness in tasks requiring extensive workspace and dexterous manipulation. In this work, we present a new class of fabric-based soft glove with 15 degrees of freedom (DOFs), including finger flexion/extension, thumb abduction/adduction, thumb opposition/reposition, and finger abduction. The high-DOF fabric-based soft glove integrates bidirectional fabric-based pneumatic actuators (FPAs) for finger flexion/extension, X-crossing pneumatic artificial muscles (X-PAMs) for thumb assistance, and Y-shaped bladed FPAs for finger abduction. To enhance the thumb tip workspace, we optimize the X-PAM positioning by modeling thumb kinematics from an anatomical perspective. The experimental results show that the optimized passive workspace of the thumb, assisted by the glove, encompasses approximately 70% of its active workspace. Through our mirror control system, we further demonstrate the glove's capability to perform complex gestures and versatile grasping tasks with various object geometries, sizes (0.1–11.5 cm), and masses (1.7–500.0 g). The glove supports both power and precision grasps, as well as fine manipulations.

Keywords: soft glove, fabric-based actuator, high DOFs, thumb assistance, wearable robots

Introduction

The human hand plays a pivotal role in both occupational tasks and activities of daily living (ADLs) owing to its exceptional dexterity. It functions not only as the primary organ for object manipulation and tool usage but also as a vital medium for communication, interaction, and emotional expression. The human hand has >20 degrees of freedom (DOFs)[1] and a complex musculoskeletal structure, forming the essential basis for its dexterous manipulation capabilities. Nevertheless, various neurological deficits, including stroke, spinal cord injury, Parkinson's disease, brachial plexus injury, and cerebral palsy, can impair hand functionality that significantly diminish patients' quality of life.[2,3] As a promising solution for rehabilitation training and daily support, robotic gloves have emerged over the past decade.[4–7]

Among robotic gloves, the conventional hand exoskeletons with rigid components, relying on linkages to transform motion, have attracted much attention due to their high output force and accurate position control.[8–10] However, their application is limited due to the complex mechanisms, substantial weight, high cost, and misalignment-caused discomfort.[11] In contrast, soft gloves demonstrate superior characteristics in compliance, safety, and economy.[2,12] Recently, many soft robotic gloves have been reported, which can be categorized into cable-driven,[13,14] elastomer-based,[15–18] and fabric-based soft gloves.[4,19–22]

In these developments, fabric-based soft gloves particularly excel in terms of light weight, portability, and flexibility,[23] exhibiting unique structural programmability (Supplementary Table S1). For instance, Correia et al.[24] present a soft glove using two thermoplastic elastomer balloons as the chambers between three fabric layers to implement finger flexion and extension. The glove showcases exceptional performance in Jebsen Taylor Hand Function Test and implements a broad range of motion (ROM) and high grasp force. Suulker et al.[25]

Robotics Institute and State Key Laboratory of Mechanical System and Vibration, School of Mechanical Engineering, Shanghai Jiao Tong University, Shanghai 200240, China.

apply an elastic band to enhance the flexion angle and force of fabric-based pneumatic actuators (FPAs), thus augmenting the performance of the integrated soft glove. Alternatively, Lai et al.[5] develop a novel honeycomb pneumatic actuator (HPA) by introducing a guide layer between two layers of a common FPA, which substantially increases the end output force by 862%. The soft glove integrating HPAs effectively facilitates ADLs on nine patients. Despite the accumulative efforts in developing fabric-based soft gloves, existing works predominantly focus on finger flexion/extension, typically involving 10 DOFs or less. They aim to increase output force while devoting limited attention to the complexity of the hand, particularly the thumb, which plays a crucial role in hand dexterity and grasping.[26–28] The absence of these thumb DOFs diminishes the gloves' ability to perform dexterous manipulations. Grasping objects with different shapes, sizes, and material properties places distinct demands on the hand gestures; nevertheless, solely relying on flexion/extension movements is deficient to meet the diverse functional requirements of real-world tasks.

To improve the dexterity of soft gloves, several attempts have been conducted with thumb assistance. For instance, some cable-driven and elastomer-based gloves are reported to realize the partial actuation of thumb opposition/reposition[6,7,29] or abduction.[30] Regarding fabric-based gloves, researchers have also attempted to incorporate specific designs for the thumb. Yap et al.[31,32] deploy a flexion actuator featuring slanted corrugates near the proximal side of the thumb, allowing concurrent bending and twisting motions, to generate more ergonomic thumb flexion. Lim et al.[33] design a thermoset plastic thumb splint to tackle the thumb misalignment with the four fingers. However, independent abduction is sacrificed when thumb opposition is simplified solely as a coupling of flexion and twisting,[34] thereby constricting the actuated workspace. Achieving independent thumb abduction/adduction and opposition/reposition remains challenging. The challenges mainly lie in: (i) replicating the extensive ROM exhibited by the human thumb joints,[34] (ii) decoupling and simplifying the multiple coupled DOFs of the thumb,[35] and (iii) arranging actuators within the narrow space surrounding the thumb without compromising function or comfort.

In this work, we present a new high-DOF fabric-based soft glove with dexterous thumb assistance. Our glove integrates three classes of actuators and achieves 15 DOFs in total, including independent finger flexion/extension, thumb abduction/adduction, thumb opposition/reposition, and finger abduction. The rest of this article is organized as follows. The Design and Optimization section details the glove design and optimization of the thumb actuator positioning based on thumb kinematics. The Workspace of the Thumb with Glove Assistance section compares the active and passive thumb tip workspace experimentally, further validating the effectiveness of the optimization. The Validation of Application Performance section presents the control system and manifests the applications of the glove in various grasping and manipulating tasks. Finally, the Discussion and Conclusion section concludes this article.

Design and Optimization

Design of fabric-based soft glove with high DOFs

The design of the high-DOF fabric-based soft glove is illustrated in Figure 1a. We deploy five high-force bidirectional FPAs with asymmetrical chambers for flexion and extension (Fig. 1b) on the five fingers. Three X-crossing pneumatic artificial muscles (X-PAMs) (Fig. 1c) and a butterfly-shaped actuator (Fig. 1d) are comprised to assist the movements of the thumb carpometacarpal (CMC) joint. They enable thumb opposition, reposition, adduction, and abduction, achieving omnidirectional thumb movements. In addition, three finger abduction actuators (Fig. 1e) are stitched between the fingers to expand the enveloping space during grasping. The soft glove embodies 15 DOFs and weighs 123.5 g in its wearable section. Its grip force attains 23.80 ± 0.51 N at 120 kPa (experimental setup detailed in Supplementary Fig. S1).

FPAs for flexion and extension. To facilitate the flexion and extension of the fingers, we employ five high-force bidirectional FPAs (Fig. 1b), presented in our previous work.[36,38] The FPA is composed of two asymmetrical chambers, with the lower chamber I designed to achieve extension through inflation. Chamber II, with a corrugated structure, is fixed onto chamber I via heat pressing. By inflating chamber II, the FPA flexes due to mutual extrusion between the adjacent pleat surfaces. We can achieve independent flexion or extension of each finger by inflating the corresponding chambers of the FPA.

Targeting suitable sizes for different fingers, we design four categories of FPAs with distinct widths, lengths, and numbers of corrugated pleats. The index and middle fingers are equipped with six-pleat FPAs, each measuring 185 mm in length, while the remaining three fingers adopt five-pleat FPAs with a length of 160 mm. To achieve a higher output force, the FPAs for the thumb and index finger feature a width of 30 mm. In contrast, the FPAs for the other three fingers prioritize lightness and portability, incorporating a width of 25 mm. The tip-blocked force of the thumb FPA reaches 8.3 ± 0.2 N at 120 kPa.[38]

X-PAMs for omnidirectional thumb assistance. Actuation of the thumb, especially the CMC joint, necessitates actuators capable of muscle-like linear contraction. X-PAMs, presented in our work,[37] play a competitive option due to their excellent performance. The working principle of the X-PAM is illustrated in Figure 1c. An X-PAM is composed of a rectangular chamber and two comb-like areas (i.e., "filaments") to achieve force and motion transmission through the X-crossing mechanism. It is capable of directly transmitting the chamber expansion into linear contraction along the actuator axis by positive pressure. Upon inflation, the air chamber expands and stiffens, altering its bending configuration, which actuates the filaments at both ends to contract along the axis. Due to the unique mechanism, the X-PAM features a considerable contraction ratio of >90% and a high output force of >200 N/kg/kPa.

Figure 1a depicts the placement of the four thumb actuators and their respective functions. Thumb assistance includes opposition, reposition, and adduction facilitated by three X-PAMs, and abduction realized by the butterfly-shaped actuator (Fig. 1d), which provides linear expansion movement (with their lengths represented with L_1–L_4 sequentially). The strokes and lengths of these four thumb actuators are customized according to the thumb dimensions of the subject, as described in Table 1. L_{k-min} and L_{k-max} represent the minimum and maximum lengths of each thumb

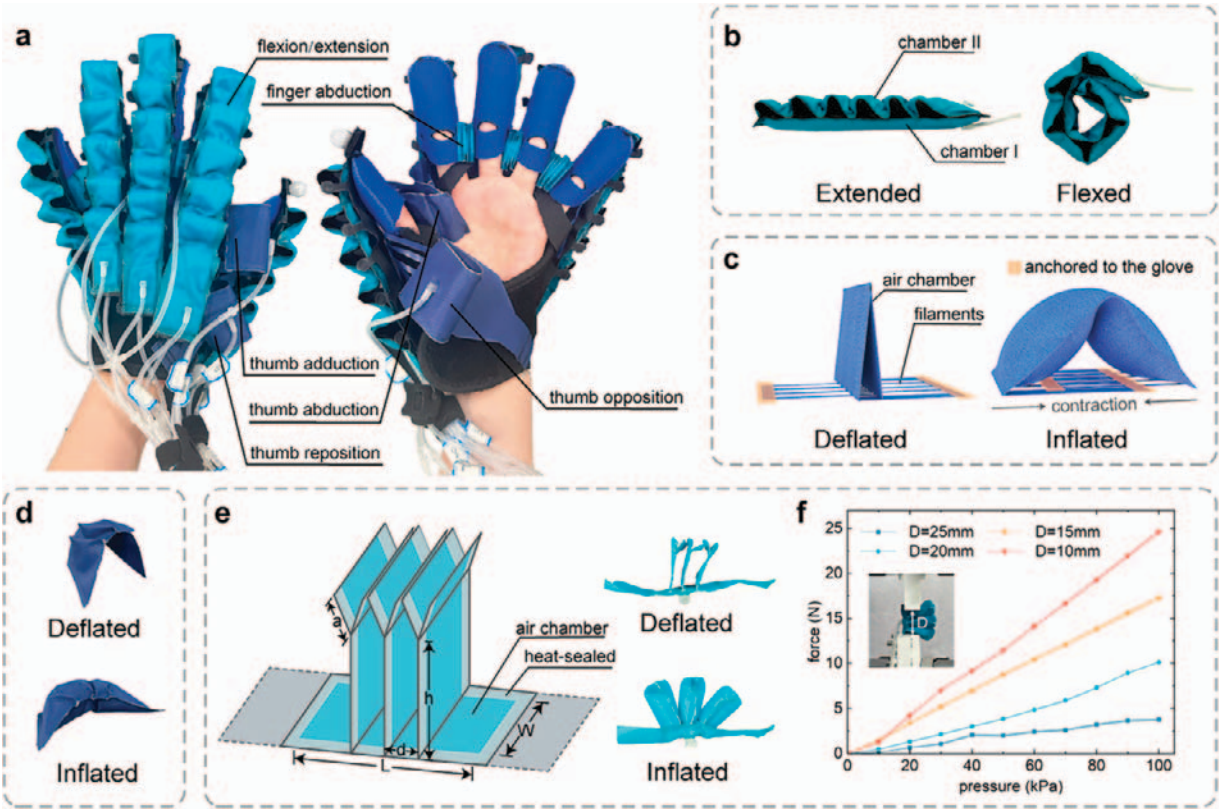

FIG. 1. Design of fabric-based soft glove with high degrees of freedom (DOFs). **(a)** The soft glove. **(b)** The bidirectional fabric-based pneumatic actuator (FPA) for flexion and extension.[36] **(c)** The X-crossing pneumatic artificial muscle (X-PAM) for thumb opposition, reposition, and adduction.[37] **(d)** The actuator for thumb abduction. **(e)** The actuator for finger abduction. **(f)** Output force–pressure relationships at different abduction distances.

actuator, respectively, and their difference (i.e., ΔL) is the designed stroke. The four thumb actuators form two antagonistic pairs and substantially cover the two DOFs of the CMC joint of the thumb,[39] thereby enabling omnidirectional assistance.

Actuators for finger abduction. Grasping objects, especially power grasps, generally requires sufficient enveloping space. In this work, we design a novel finger abduction actuator featuring interconnected Y-shaped chambers (Fig. 1e). When deflated, the three chambers flatten to occupy minimum volume, thus not affecting the natural adduction of the fingers. Upon inflation, the chambers expand to enable finger abduction movement. The blades of the actuator ensure that the distal air chamber expands wider than the proximal end, effectively securing the actuator between the fingers. Geometric parameters of the finger abduction actuator presented in Figure 1e are as follows: $L = 20$ mm, $W = 18$ mm, $a = 5$ mm, $h = 16$ mm, $d = 5$ mm, and the seam width of heat-sealing is 3 mm. The three abduction actuators with the same parameters are positioned between the four fingers, as illustrated in Figure 1a.

TABLE 1. STROKES AND LENGTHS OF THUMB ACTUATORS

	L_1	L_2	L_3	L_4
$\Delta L/mm$	75	40	60	105
L_{k-min}/mm	85	90	30	30
L_{k-max}/mm	160	130	90	135

We characterize the force–pressure relationships of the finger abduction actuators. To simulate the pinching action between the fingers, we introduce two rectangular panels to constrain the actuator during characterization. Besides, the dimensions of the two panels are based on the actual contact area between the subject's fingers and the actuator. The distance between the panels (D) is set at 10, 15, 20, and 25 mm, encompassing the abduction distance range of 15–20 mm obtained from the human hands. Pressure applied to the testing actuator varies from 0 to 100 kPa in increments of 10 kPa. These steps are repeated on the three abduction actuators with the same parameters, each conducted three times. The characterization results of the output force are presented in Figure 1f, demonstrating an approximately linear relationship between the output force and the pressure.

When integrated into a soft glove, the actuators enable a considerable fraction of the ROM of human finger abduction. We measure the active and passive finger abduction angles of the subject before and after actuating the glove. Each test is conducted three times for reliability. The experimental outcomes show that the active abduction angle averages $26.11° \pm 0.96°$, while the passive abduction angle, assisted by the glove, is $22.46° \pm 0.24°$. Incorporation of the finger abduction actuators enables the soft glove to achieve >86% of the active ROM.

Optimization of X-PAM positioning

Kinematics of the thumb. To enlarge the glove-assisted thumb workspace, we establish a model to optimize the positioning of the three X-PAMs. The anchoring position of the butterfly-shaped thumb abduction actuator is fixed due to spatial constraints near the index finger.

The arrangement of the actuators is illustrated in Figure 2a. Four thumb actuators, represented by wavy lines, are anchored at point C on the thumb, with their opposite ends sewn to specific regions on the glove (A_1, A_2, and A_3 for the X-PAMs corresponding to thumb opposition, reposition, and adduction, respectively, while A_4 for the thumb abduction actuator). In the model, they are simplified into variable-length rods with determined strokes, denoted as CA_1–CA_4. The dorsal and palmar sides of the hand are modeled as two parallel planes with a distance of the palm thickness. The rectangular areas at A_1–A_3 represent the optimization domains for X-PAM positioning, while point C remains fixed relative to the thumb during optimization.

The origin of the Cartesian coordinate system is located at the CMC joint of the thumb, with the y-axis aligned with the extended index finger and the z-axis perpendicular to the palm. The kinematics of the thumb are derived from anatomical foundations and further simplified for analytical purposes.[39] As depicted in Figure 2b, the thumb is modeled as a three-link mechanism. The CMC joint is modeled as a

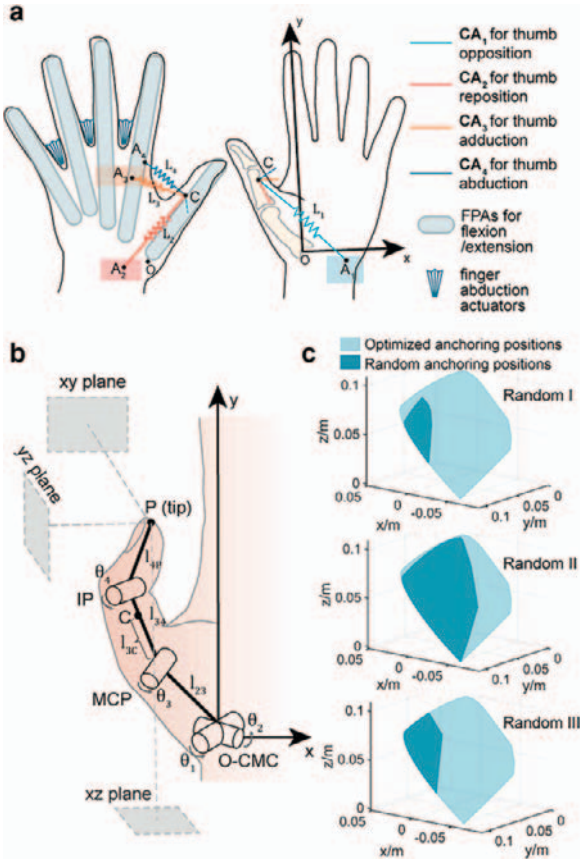

FIG. 2. Parameter optimization of the soft glove. **(a)** Actuator layout and optimization domains. **(b)** Kinematics of the thumb. **(c)** Workspace comparison of optimized and randomly generated anchoring positions.

Cardan joint with two DOFs, and the two rotary axes are perpendicular to each other, corresponding to flexion/extension and abduction/adduction, decoupled from real thumb movements. Unlike the other four digits, the flexion/extension axis of the thumb's CMC joint is not parallel to the palm but is angled according to anatomical studies (a divergent angle of 30°, followed by a spin angle of 45°),[40,41] as shown in Eq. (1). Variables for these two DOFs are denoted as θ_1 and θ_2. Meanwhile, the metacarpophalangeal (MCP) and interphalangeal (IP) joints are modeled as rotation joints, each with one DOF, represented as θ_3 and θ_4, respectively. The lengths of the three phalanges are represented as l_{23}, l_{34}, and l_{4P} sequentially. The distance between the fixed point C and the MCP joint is denoted as l_{3C}.

Under these assumptions, we can represent the coordinates of the thumb tip with respect to the base coordinate system through Denavit–Hartenberg theory[42] and homogeneous coordinate transformation matrices. The specific transformation matrices are detailed as follows:

$$ {}^{base}_{0}\mathbf{T} = \begin{bmatrix} 0 & -\sin30^\circ & \cos30^\circ & 0 \\ 0 & \cos30^\circ & \sin30^\circ & 0 \\ -1 & 0 & 0 & 0 \\ 0 & 0 & 0 & 1 \end{bmatrix} \begin{bmatrix} \cos45^\circ & 0 & \sin45^\circ & 0 \\ 0 & 1 & 0 & 0 \\ -\sin45^\circ & 0 & \cos45^\circ & 0 \\ 0 & 0 & 0 & 1 \end{bmatrix} \tag{1} $$

$$ {}^{0}_{1}\mathbf{T} = \begin{bmatrix} \cos\theta_1 & -\sin\theta_1 & 0 & 0 \\ \sin\theta_1 & \cos\theta_1 & 0 & 0 \\ 0 & 0 & 1 & 0 \\ 0 & 0 & 0 & 1 \end{bmatrix} {}^{1}_{2}\mathbf{T} = \begin{bmatrix} 0 & 0 & 1 & 0 \\ -\sin\theta_2 & \cos\theta_2 & 0 & 0 \\ -\cos\theta_2 & -\sin\theta_2 & 0 & 0 \\ 0 & 0 & 0 & 1 \end{bmatrix} $$

$$ {}^{2}_{3}\mathbf{T} = \begin{bmatrix} 0 & 0 & 1 & 0 \\ -\sin\theta_3 & \cos\theta_3 & 0 & l_{23} \\ -\cos\theta_3 & -\sin\theta_3 & 0 & 0 \\ 0 & 0 & 0 & 1 \end{bmatrix} {}^{3}_{4}\mathbf{T} = \begin{bmatrix} \cos\theta_4 & \sin\theta_4 & 0 & 0 \\ -\sin\theta_4 & \cos\theta_4 & 0 & l_{34} \\ 0 & 0 & 1 & 0 \\ 0 & 0 & 0 & 1 \end{bmatrix} \tag{2a-2d} $$

Thus, the position of the thumb tip, denoted as P, can be expressed as

$$ P = {}^{base}_{0}\mathbf{T}\,{}^{0}_{1}\mathbf{T}\,{}^{1}_{2}\mathbf{T}\,{}^{2}_{3}\mathbf{T}\,{}^{3}_{4}\mathbf{T} \begin{bmatrix} 0 \\ l_{4P} \\ 0 \\ 1 \end{bmatrix} \tag{3} $$

Similarly, the fixed point C can be denoted as

$$ P_C = {}^{base}_{0}\mathbf{T}\,{}^{0}_{1}\mathbf{T}\,{}^{1}_{2}\mathbf{T}\,{}^{2}_{3}\mathbf{T} \begin{bmatrix} 0 \\ l_{3C} \\ 0 \\ 1 \end{bmatrix} \tag{4} $$

Optimization and results. We aim to find a set of anchoring positions of the X-PAMs (A_1–A_3) to maximize the thumb tip workspace. To further define the workspace of the thumb tip, a projection-based convex hull method is conducted with the following steps. With a specific group of joint angles of the thumb, the vector $\boldsymbol{\theta}$ is expressed as

$$\boldsymbol{\theta}^{(\cdot)} = [\theta_1\ \theta_2\ \theta_3\ \theta_4] \tag{5}$$

Thereby, we yield the position of the thumb tip (point P) and the fixed point C according to Eqs. (3) and (4), presented as

$$P^{(\cdot)} = f_P(\boldsymbol{\theta}) \tag{6}$$

$$P_C^{(\cdot)} = f_C(\boldsymbol{\theta}) \tag{7}$$

We traverse the ROM of the four joint angles, attaining the point set reachable by the thumb tip as

$$\mathcal{S}_P = \{\{P^{(1)}, P^{(2)}, P^{(3)}, ...\} \mid P^{(\cdot)} = f_P, P_C^{(\cdot)} = f_C \in \mathcal{C}, \boldsymbol{\theta} \in \Theta\} \tag{8}$$

where $\mathcal{C}$ and Θ represent the constraint conditions for the actuator lengths and joint angles, respectively: (i) The lengths of the four thumb actuators (L_k) must remain within the designed stroke range, customized for the subject's hand (see Fig. 2a and Table 1). (ii) The ROM of the four joint angles is within the constraints of human physiology (Table 2).[43,44] We quantify these constraint conditions as

$$\mathcal{C} = \{P_C \mid L_k \in [L_{k-min}, L_{k-max}], k = 1,2,3,4\} \tag{9}$$

$$\Theta = \{\boldsymbol{\theta} \mid \theta_l \in [\theta_{l-min}, \theta_{l-max}], l = 1,2,3,4\} \tag{10}$$

We then project the point set $\mathcal{S}_P$ onto three orthogonal planes of the Cartesian coordinate system, as illustrated in Figure 2b. The projected point sets are

$$\mathcal{S}_{P_{ij}} = proj_{ij}(\mathcal{S}_P), i,j \in \{X,Y,Z\}, i \neq j \tag{11}$$

We calculate the convex hull areas for each $\mathcal{S}_{P_{ij}}$.[45] The sum of these three areas is set as the optimization objective function, which is

$$g(A_1,A_2,A_3) = \sum_{i,j\in\{X,Y,Z\}}^{i\neq j} Area\left(ConvexHull(\mathcal{S}_{P_{ij}})\right) \tag{12}$$

Due to the planar assumption of the dorsal and palmar sides of the hand, the optimization domains of A_1–A_3 are rectangular areas parallel to the XY plane, while A_4 is fixed relative to the glove at (30, 85, 0), as indicated in Table 3. These areas are distant from the CMC joint of the thumb, thereby remaining approximately planar during thumb motions. The selections of the optimization domains simultaneously ensure that the thumb actuators are all mountable on the glove without interfering with each other. The constraints of the anchoring positions are expressed as

$$A_k \in \{(x,y,z_k) \mid x_{k-min} \leq x \leq x_{k-max}, y_{k-min} \leq y \leq y_{k-max}\}, k = 1,2,3,4 \tag{13}$$

Additionally, the phalange lengths are fixed values measured from the subject: l_{23} = 43 mm, l_{34} = 36 mm, l_{4P} = 37 mm, and l_{3C} = 27 mm. It should be noted that the hand dimensions necessitate re-measurement for different subjects, including determining the phalange lengths and the optimization domains (A_1–A_4).

We then employ the Particle Swarm Optimization (PSO) algorithm in MATLAB (MathWorks Inc., USA) to calculate the anchoring positions that maximize the workspace. Taking all the above conditions into account, we determine the optimal anchoring positions to be A_1 (80, –40, 25), A_2 (38, –35, 0), and A_3 (30, 45, 0). In addition, the results show that the optimal positions of A_1 are distributed across a certain region. To prevent the actuator from being too close to the palm and impeding full-hand grasping, the most distal position is selected. Subsequent trials confirm that the positioning of the actuators does not interfere with grasping.

To validate the effectiveness of the optimization, we generate three additional groups of anchoring positions for the X-PAMs randomly and compute their optimization function values (Table 4). Their corresponding thumb tip workspace configurations are shown in Figure 2c, compared with the optimized group. The results indicate that the positions optimized by the PSO algorithm significantly enhance the thumb workspace.

Table 2. ROM of Four Joint Angles Based on Human Physiology[43,44]

	θ_1	θ_2	θ_3	θ_4
θ_{l-min}/°	0	0	0	0
θ_{l-max}/°	40	45	50	80

ROM, range of motion.

Table 3. Optimization Domains of Anchoring Positions

	A_1	A_2	A_3	A_4
X/mm	[60, 100]	[30, 70]	[30, 80]	30
Y/mm	[−40, −10]	[−35, −15]	[45, 65]	85
Z/mm	25	0	0	0

Workspace of the Thumb with Glove Assistance

We apply the above optimization method to guide the design of the high-DOF fabric-based soft glove. To evaluate the glove's performance in replicating human thumb movements, we conduct a comparative analysis of the passive and active workspace of the thumb tip. This comparison also validates the optimization.

Experimental setup and methods

We deploy a 3D optical motion tracking system (Prime 13, OptiTrack, USA) to measure the workspace of the thumb tip. The experimental setup is depicted in Figure 3a. Measurements are conducted with and without the glove actuated under identical conditions. A total of five cameras are utilized to minimize the risk of missing markers. During testing, the subject sits comfortably at the desk, with the elbow and part of the wrist secured in a jig, using nonelastic Velcro straps to prevent any wrist movement. The forearm and wrist are consistently positioned, with the thumb oriented upward.

Two reflective markers are attached to the glove, with one located at the thumb tip and the other adjacent to the CMC joint to mark the origin (Fig. 3b). Informed consent from the subject is obtained.

The process for measuring the thumb's active workspace without glove actuation involves three steps (Fig. 3c): (i) with the MCP and IP joint fully extended, the CMC joint rotates to allow the thumb tip to trace the largest circle, denoted as Set I. (ii) With the MCP and IP joint in maximum flexion, the CMC joint rotates to trace another large circle, denoted as Set II.[46] (iii) The thumb moves randomly within a 60-s time limit to generate a dense point set, denoted as Set III. The sampling frequency is 20 Hz, and these three point sets are combined to determine the active workspace.

Subsequently, the thumb's passive workspace is obtained by actuating the soft glove with a predefined air pressure sequence. This test involves six air chambers, four from the actuators for thumb opposition/reposition and abduction/adduction and two from the bidirectional FPA for thumb flexion/extension. The pressure sequence consists of two parts: (i) pressure combinations assigned to six chambers by traversing all possibilities under three pressure levels (0, 50, and 100 kPa) and (ii) supplementary combinations at the limit positions of thumb movement (i.e., the edges of the achievable space). This part is achieved by varying the pressures of CA_1 and CA_2 from 0 to 100 kPa in increments of 10 kPa while maintaining the thumb in full extension and abduction. This approach enhances the accuracy of the convex hull area computation. To reduce the influence of involuntary muscle activation, the tests are repeated three times with a rest interval imposed after each trial.

Results

Workspace comparison of active thumb motion and passive actuation in the 3D view is demonstrated in Figure 3d. We apply an identical method to calculate the projected workspace, as described in the optimization process. The results of the projected workspace are shown in Figure 3e, demonstrating that the thumb, assisted by the soft glove, can cover $70.3 \pm 1.1\%$, $76.3 \pm 1.5\%$, and $63.7 \pm 5.0\%$ of the active workspace on the *XY*, *XZ*, and *YZ* planes, respectively. The calculation of these ratios during passive actuation excludes points (i.e., the yellow points in Fig. 3e) that exceed the active workspace. Despite the removal of these points, the glove covers a substantial portion of the active workspace and has a considerable impact on assisting the thumb in moving through a sufficiently large space.

Validation of Application Performance

Mirror control system

To validate the practical performance of the optimized soft glove in assisting hand movement and grasping, we implement a mirror actuation control strategy. This approach involves capturing the movements of the contralateral hand as input signals to precisely control the glove-assisted hand via a pneumatic system, enabling the desired gestures. Because we connect the three finger abduction actuators in parallel, a total of 15 air channels are required, corresponding to the 15 DOFs of the glove. While high DOFs increase the complexity of pneumatic control, vision-based capture technology mitigates the strain sensor placement challenges caused by DOF coupling, improving stability.

The control system setup is illustrated in Figure 4. We utilize a vision-based motion capturing system (Leap Motion, Ultraleap, USA) to collect joint position data from the contralateral hand as the input. The open-source MatLeap interface in MATLAB (MathWorks Inc., USA) enables us to receive the data from the Ultraleap software program. The captured joint positions are processed to derive phalange and palm vectors, from which the joint angles are subsequently calculated. These angles are then mapped to the corresponding pressure of each air channel, as shown in Table 5. For simplicity and control stability, all mapping relationships are defined as linear. Employing the motion capturing system, we record the angular range of each DOF from the contralateral hand and linearly map it to the required pressure range of the corresponding actuator. Minor adjustments are made to better ensure that the glove achieves a satisfactory reproduction of the contralateral hand's movements (Table 5).

The calculated air pressure signals are sent via Ethernet serial ports to a dSPACE control box (microLabBox 1202, dSPACE, Germany), driving the pressure regulators to supply the designated pressures to the glove. The air compressor (ED-0204, Eidolon, China) serves as the pressure source for all channels. This system allows us to adjust the pressure values in real time based on the captured hand gestures. The system latency from joint position acquisition to gesture replication stabilizes within 0.7 s after sustained use.

Basic movement of each DOF

Through mirror actuation, the glove-assisted hand performs a variety of basic movements, as demonstrated in Figure 5 and Supplementary Movie S1. Each bidirectional FPA can be actuated to present the flexed or extended state independently, enabling a series of gestures, including hand opening and closing (Fig. 5a). Three Y-shaped bladed FPAs realize finger abduction, allowing adjustments to the enveloping space during grasping (Fig. 5b). Besides, the glove supports independent thumb abduction/adduction and opposition/reposition (Fig. 5c and d). The antagonistic relationships of the thumb actuators enable the thumb to perform circular motion around the CMC joint (Fig. 5e). The glove further enables various compound gestures (Fig. 5f). Transitions between the gestures are smooth, supported by the mirror control strategy. The basic movements accomplished above serve as compelling evidence for the effectiveness of the soft glove.

Grasping and manipulation

We conduct a series of grasping and manipulation tasks to assess the application capabilities of the high-DOF soft glove (see Figs. 6–8, Supplementary Fig. S3, and Supplementary Movie S2). Supplementary Figure S2 and Supplementary Table S2 present the complete object set, along with the corresponding dimensional and mass specifications. The grasped objects are judiciously selected to exhibit pronounced diversity in dimensions, weights, geometries, stiffness, and surface texture. As demonstrated in Figure 6 and Supplementary Figure S3, the test set contains geometric

Table 4. Comparison of Randomly Generated and Optimized Anchoring Positions

(x, y)	A_1/mm	A_2/mm	A_3/mm	Function value/mm^2
Random I	(85.29, −37.07)	(35.08, −16.73)	(70.74, 63.12)	6009.63
Random II	(60.30, −10.88)	(68.30, −15.70)	(43.92, 55.94)	19983.78
Random III	(93.97, −11.98)	(56.23, −34.29)	(69.61, 64.19)	9819.80
Optimized	(80, −40)	(38, −35)	(30, 45)	25350.82

items from the Action Research Arm Test,[47] such as wooden blocks of different dimensions (2.5 cm and 7.5 cm), a wooden ball (Φ7.5 cm), and steel tubes (Φ1 cm, shown in Fig. 7b, and Φ2.25 cm). For irregular and deformable objects relevant to ADLs, we accomplish grasping a hand model, a flexible milk package, and a bunch of artificial grapes. Through mirror control, appropriate gestures are adopted to grasp geometrically extreme objects, for example, pinching a slender flower and laterally gripping a thin disc. Moreover, we can pick up and hold a pen with a writing tripod gesture.

Figures 7 and 8 further highlight the glove's versatility in gripping objects with multiple gestures and performing manipulations. As illustrated in Figure 7a, the glove can assist in gripping a steel bowl using both envelope grasping and edge pinching. When grasping a thin steel tube with a small diameter (1 cm), the soft glove performs a variety of grasping and pinching motions. Figure 7b displays scenarios where the glove is utilized for a full grasp with the thumb extended, along with two-finger pinching using the thumb and the other three fingers separately. Additionally, the comprehensive integration of multiple actuators enables the soft glove to execute the entire procedure of picking up a thin card from a flat surface (Fig. 7c).

To further demonstrate the glove's capability for fine manipulation, we rotate a silicone ball with three fingers both clockwise and counterclockwise (see Fig. 8 and Supplementary Movie S3). The rotation consistently achieves an angle of approximately 60°, as shown in Figure 8a. The recorded control pressure sequences confirm that the pneumatic system effectively adjusts the pressure of the corresponding chambers through mirror actuation. As illustrated in Figure 8a, the primary DOFs involved in this task are thumb opposition/reposition and flexion/extension, while the index and middle fingers mainly provide passive support, resulting in minimal variations in the pressure sequences of their corresponding actuators.

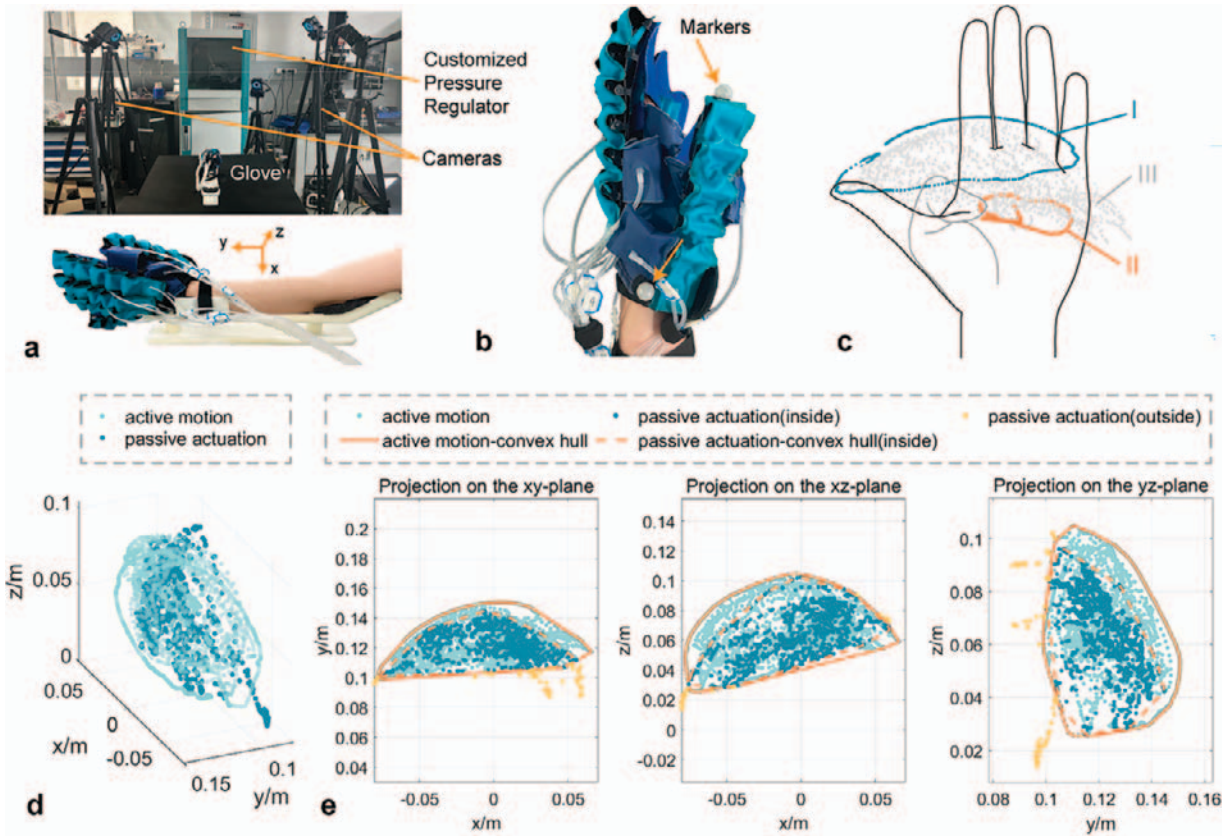

FIG. 3. Workspace of the thumb with a high-DOF fabric-based soft glove. **(a)** Experimental setup. **(b)** The arrangement of markers. **(c)** The active moving trajectory of the thumb with pneumatic actuation OFF. **(d)** Workspace comparison of active thumb motion and passive actuation in the three-dimensional view. **(e)** Workspace comparison of active thumb motion and passive actuation projected onto three orthogonal planes.

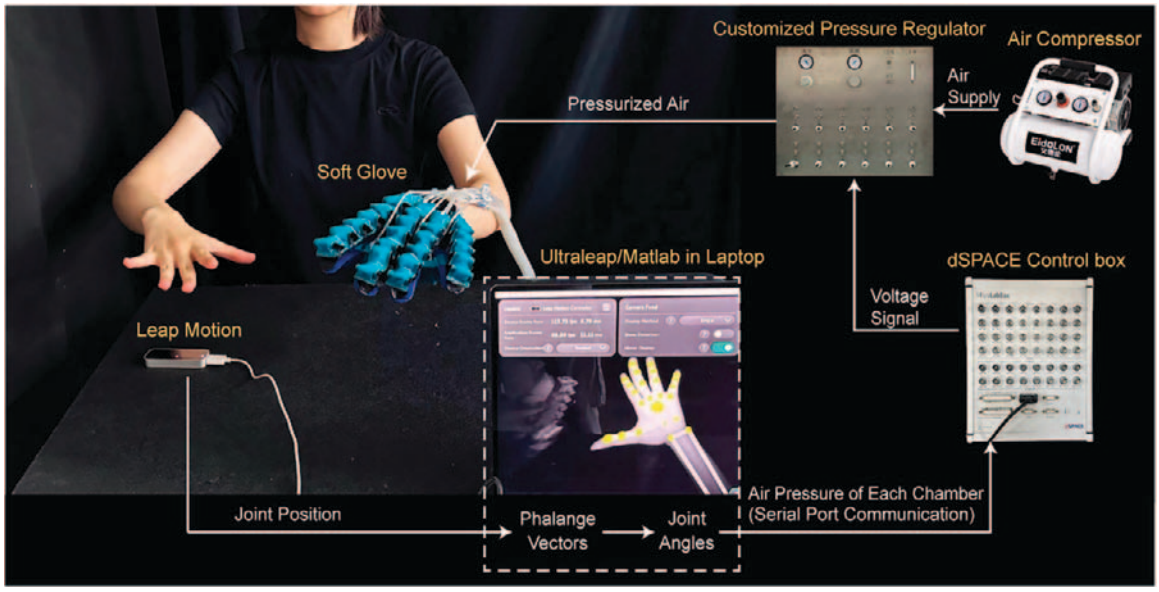

FIG. 4. Control system of mirror actuation of the soft glove.

During the task, three electrodes are attached to the skin after it is cleaned with alcohol pads. The electrodes are placed over the abductor pollicis longus, extensor pollicis longus, and flexor digitorum superficialis to monitor muscle activity using an electromyography (EMG) system (Trigno Wireless EMG System, DELSYS Inc., USA), as shown in Figure 8b. To extract the EMG envelope, a sequential signal processing pipeline is employed, including band-pass filtering (0.1–500 Hz), 50 Hz notch filtering to remove power line interference, full-wave rectification, and low-pass filtering at 5 Hz for signal smoothing.[38] We compare the normalized EMG amplitudes (relative to the subject's maximum voluntary contraction, which is measured by exerting maximal effort during contractions in the corresponding direction for each muscle group) of both glove-assisted rotation and freehand active rotation (i.e., without glove assistance). Under glove assistance, the EMG amplitudes of the extensor pollicis longus and flexor digitorum superficialis are significantly reduced, with noticeable decreases in signal fluctuations compared with freehand active rotation, indicating that the subject does not exert active force. The reduction in the amplitude of the abductor pollicis longus is minimal, which can be attributed to its deep anatomical location, with the signals partially obscured by the overlying extensor digitorum.

To summarize, the soft glove demonstrates satisfactory performance across a wide range of grasping and manipulation tasks, effectively handling objects spanning from large, rigid items to small, delicate, and flexible objects. These grasped items vary significantly in size (0.1–11.5 cm), mass (1.7–500.0 g), and geometry, with the aspect ratios (i.e., the ratio of the longest to shortest dimensions of the object) ranging from 1.0 to 200.0, demonstrating the broad applicability of the glove. Moreover, the achieved grasping gestures embody a variety of human grasp categories, including cylindrical and spherical grasps within power grasps, as well as pinch and tripodal grasps within precision grasps.[48] Fine manipulations, such as rotating a silicone ball, highlight the dexterity of the thumb assistance.

TABLE 5. MAPPING OF JOINT ANGLES AND AIR PRESSURES

Actuator	*Function*	*Pressure–angle relationships/kPa-°*
FPAs for flexion/extension	Thumb flexion	$p = -20 + 2\theta_{MCP+IP}$
	Thumb extension	$p = 100 - 2\theta_{MCP+IP}$
	Index, middle, ring, and little finger flexion	$p = -20 + \theta_{MCP+PIP+DIP}$
	Index, middle, ring, and little finger extension	$p = 100 - \theta_{MCP+PIP+DIP}$
Abduction actuators	Finger abduction	$p = -5 + 2\theta_{finger\ abduction}$
X-PAM (CA_1)	Thumb opposition	$p = -20 + \frac{110}{90}(\theta_{opposition} - 30)$
X-PAM (CA_2)	Thumb reposition	$p = 100 - \frac{110}{90}(\theta_{opposition} - 30)$
X-PAM (CA_3)	Thumb adduction	$p = 100 - 2.5(\theta_{thumb\ abduction} - 10) - \frac{100}{90}(\theta_{opposition} - 30)$
Abduction actuator (CA_4)	Thumb abduction	$p = -40 + 4(\theta_{thumb\ abduction} - 20)$*

*Note: If $\theta_{opposition} > 70°$, $p = -20$ kPa. This is for avoiding interference during the thumb opposition movement.
FPA, fabric-based pneumatic actuator; X-PAM, X-crossing pneumatic artificial muscle.

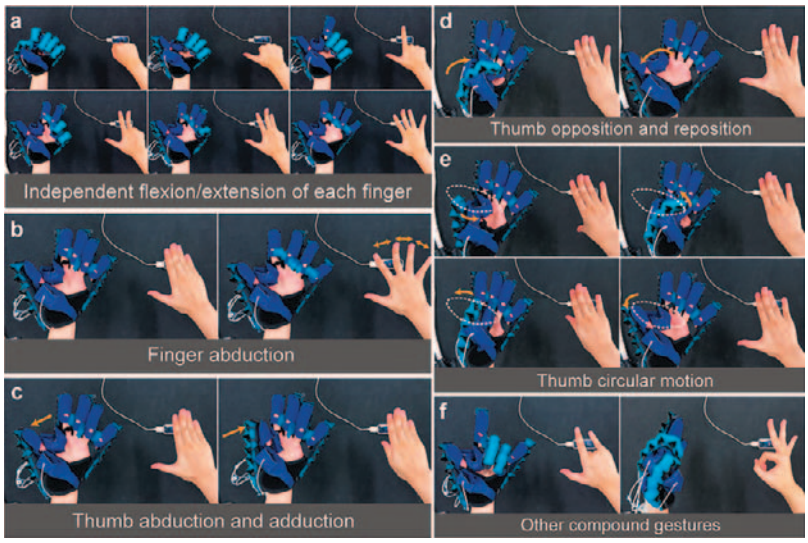

FIG. 5. Basic movements with a high-DOF fabric-based soft glove by mirror actuation. **(a)** Five bidirectional FPAs enable the independent flexion/extension of each finger. **(b)** Three Y-shaped bladed FPAs realize finger abduction. **(c)** CA_3 and CA_4 facilitate thumb abduction/adduction. **(d)** CA_1 and CA_2 implement thumb opposition/reposition. **(e)** Thumb actuators enable the circular motion of the thumb around the carpometacarpal (CMC) joint. **(f)** Integrated actuation realizes compound gestures.

Discussion and Conclusion

Focusing on enhancing the dexterity of soft gloves, we present a high-DOF fabric-based soft glove with 15 DOFs in total. The glove incorporates three classes of actuators to achieve the intricate movements mimicking the human hand. By introducing X-PAMs and optimizing their positioning based on the kinematics of the thumb, the glove implements omnidirectional thumb movements. According to the experimental results, the passive workspace of the thumb tip can reach approximately 70% of the active workspace of a human hand, significantly improving thumb assistance. Moreover, our glove features finger abduction actuation, which enhances the enveloping space during grasping. Through mirror actuation, the glove demonstrates independent control over each of its 15 DOFs and executes complex compound gestures with smooth transitions. During grasping tests, the glove facilitates the grasps of objects with various properties and realizes fine manipulation, supporting both power grasps and precision grasps. The high-DOF soft glove showcases its versatility in assisting hand movements and grasping across a wide spectrum of applications.

The presented soft glove distinguishes itself from prior designs due to its high DOFs, especially the decoupled actuation of thumb movement, and its optimization method of actuator positioning. Typically, elastomer-based gloves can achieve thumb opposition via a segmented pneumatic chamber design. Polygerinos et al.[15] employ an actuator that

FIG. 6. Grasping objects with designated gestures. The selected objects span a broad spectrum from lightweight to heavy and from compliant to rigid.

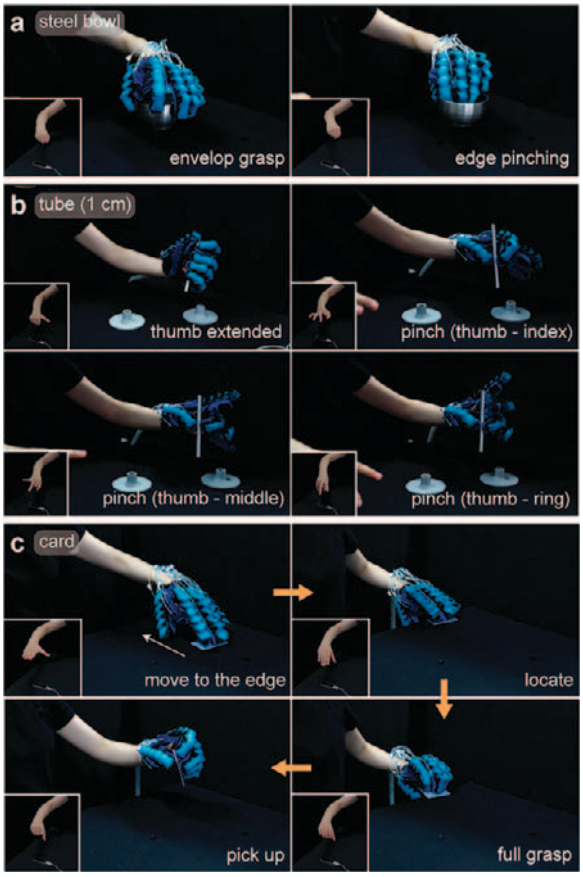

FIG. 7. Grasping with various gestures and manipulating objects. **(a)** Grasping a steel bowl. **(b)** Grasping a steel tube. **(c)** Picking up a thin card.

bends and twists around the thumb CMC joint, facilitating grasp assistance. While the glove affords effective opposition motion and simplifies control, coupling thumb flexion with opposition constrains both the workspace and dexterity. Compared with elastomer-based gloves, fabric-based gloves are more lightweight and flexible. Supplementary Table S1 compares our glove with prior representative fabric-based gloves in actuator design, force output, and grasping capabilities. Although prior works excel in distinct aspects, the presented glove exhibits remarkable advantages in high DOFs and dexterous thumb assistance. Moreover, rather than a button interface typically used for intention control, our mirror control system frees actuation from fixed modes and modulates each finger's motion in real time, accommodating diverse grasping scenarios.

However, certain limitations remain at this stage. To preserve architectural simplicity, sensors are omitted from the glove. Consequently, the open-loop control scheme increases the angular offset between the glove and the contralateral hand. Alternatively, the high-DOF characteristic of the glove renders a bulky control system, and the spatial arrangement of multiple actuators enlarges its profile, restricting the glove's home-based applicability and its usage in confined spaces. Besides, user variability in hand dimensions and kinematics necessitates a customized design to achieve optimal performance, thereby compromising universality. To demonstrate the glove's assistive efficacy across an expanded user cohort, experiments encompassing both healthy and impaired subjects are imperative in the future.

In conclusion, our high-DOF fabric-based soft glove represents a significant advancement in providing dexterous hand movement assistance. Future work will focus on: (i) reducing the glove's profile and integrating a more compact control system to improve portability and usability; (ii)

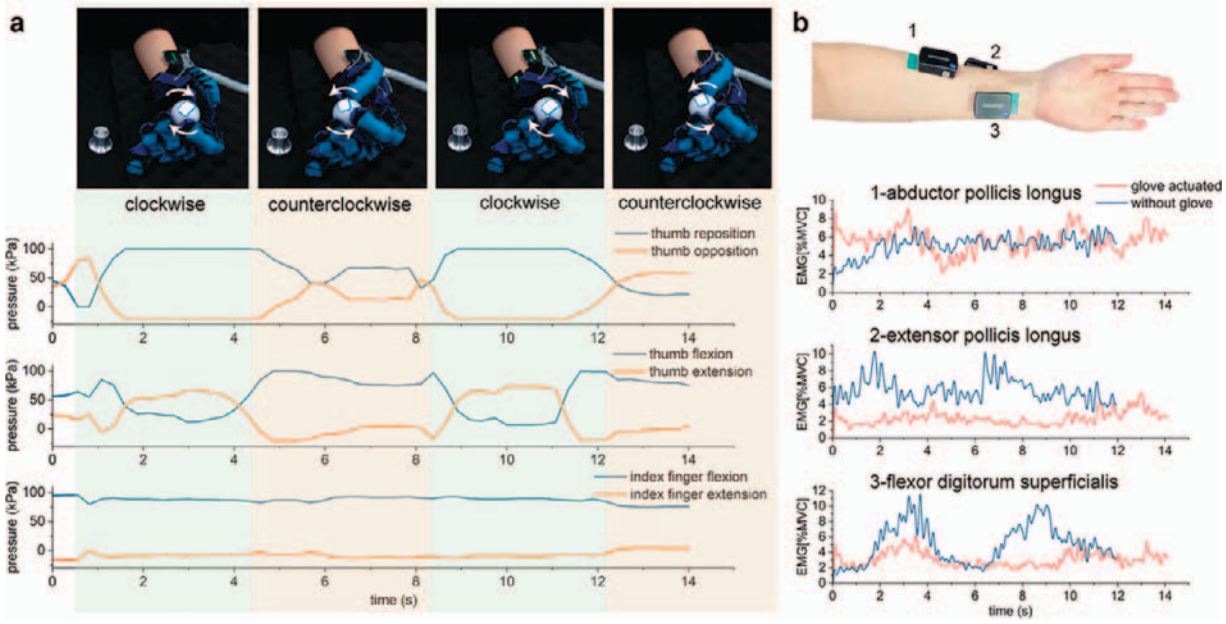

FIG. 8. Rotating a silicone ball (Φ4.3 cm, 49.3 g) clockwise and counterclockwise. **(a)** The rotating process and the corresponding control pressure sequence of the primary actuators. **(b)** The distribution of electromyographic electrodes on the skin and the EMG signals with and without the soft glove. Note: Φ-Characteristic diameter. EMG, electromyography; MVC, maximum voluntary contraction.

augmenting the pneumatic response speed by enhancing hardware performance and refining the system design; (iii) optimizing the kinematic model by accounting for factors such as soft tissue deformation, expanding the selection of parameters to be optimized, and further improving the workspace; (iv) introducing sensors on the soft glove and applying a closed-loop control to enable precise angle mirroring; and (v) deploying the soft glove for patient trials to improve its usage effectiveness and user experience.

Acknowledgments

The authors thank Y. Rong, Z. Yuan, and X. Shi for their help with data collection related to workspace measurements and X. Yang for his suggestions on the model establishment.

Authors' Contributions

J.S. and M.F. conceived the idea and developed the model for optimization. J.S., M.F., and D.Y. performed the experiments and analyzed the experimental data. M.F. provided the experimental setup of the motion-capturing system. G.G. supervised the project. J.S., M.F., D.Y., Y.W., and G.G. prepared the article. All the authors provided feedback and agreed to the final version of the article.

Author Disclosure Statement

No competing financial interests exist.

Funding Information

This work was supported in part by the National Natural Science Foundation of China (Grant No. 52025057), National Key R&D Program of China (Grant No. 2024YFB4707504), Science and Technology Commission of Shanghai Municipality (Grant No. 24511103400), and Xplorer Prize.

Supplementary Material

Supplementary Material
Supplementary Video S1
Supplementary Video S2
Supplementary Video S3

References

1. Feix T, Romero J, Schmiedmayer H-B, et al. The GRASP taxonomy of human grasp types. IEEE Trans Human-Mach Syst 2016;46(1):66–77; doi: 10.1109/THMS.2015.2470657
2. Chu C-Y, Patterson RM. Soft robotic devices for hand rehabilitation and assistance: A narrative review. J Neuroeng Rehabil 2018;15(1):9; doi: 10.1186/s12984-018-0350-6
3. Gopal A, Hsu W-Y, Allen DD, et al. Remote assessments of hand function in neurological disorders: Systematic review. JMIR Rehabil Assist Technol 2022;9(1):e33157; doi: 10 .2196/33157
4. Chen Y, Tan X, Yan D, et al. A composite fabric-based soft rehabilitation glove with soft joint for dementia in Parkinson's disease. IEEE J Transl Eng Health Med 2020;8: 1400110; doi: 10.1109/JTEHM.2020.2981926
5. Lai J, Song A, Wang J, et al. A novel soft glove utilizing honeycomb pneumatic actuators (HPAs) for assisting activities of daily living. IEEE Trans Neural Syst Rehabil Eng 2023;31:3223–3233; doi: 10.1109/TNSRE.2023.3302612
6. Kim DH, Lee Y, Park H-S. Bioinspired high-degrees of freedom soft robotic glove for restoring versatile and comfortable manipulation. Soft Robot 2022;9(4):734–744; doi: 10.1089/soro.2020.0167
7. Tran P, Jeong S, Lyu F, et al. FLEXotendon glove-III: Voice-controlled soft robotic hand exoskeleton with novel fabrication method and admittance grasping control. IEEE/ASME Trans Mechatron 2022;27(5):3920–3931; doi: 10.1109/ TMECH.2022.3148032
8. Sandoval-Gonzalez O, Jacinto-Villegas J, Herrera-Aguilar I, et al. Design and development of a hand exoskeleton robot for active and passive rehabilitation. Int J Adv Robot Syst 2016;13(2):66; doi: 10.5772/62404
9. Triolo ER, BuSha BF. Design and experimental testing of a force-augmenting exoskeleton for the human hand. J Neuroeng Rehabil 2022;19(1):23; doi: 10.1186/s12984-022-00997-6
10. Xu W, Guo Y, Bravo C, et al. Design, control, and experimental evaluation of a novel robotic glove system for patients with brachial plexus injuries. IEEE Trans Robot 2023;39(2):1637–1652; doi: 10.1109/TRO.2022.3220973
11. Xiloyannis M, Alicea R, Georgarakis A-M, et al. Soft robotic suits: State of the art, core technologies and open challenges. IEEE Trans Robot 2022;38(3):1343–1362; doi: 10.1109/TRO.2021.3084466
12. Billard A, Kragic D. Trends and challenges in robot manipulation. Science 2019;364(6446):eaat8414; doi: 10.1126/ science.aat8414
13. Lee Y, Park H-S. Design optimization of a soft robotic rehabilitation glove based on finger workspace analysis. Biomimetics (Basel) 2024;9(3):172; doi: 10.3390/biomimetics9030172
14. Tran P, Elliott D, Herrin K, et al. Towards comprehensive evaluation of the FLEXotendon glove-III: A case series evaluation in pediatric clinical cases and able-bodied adults. Biomed Eng Lett 2023;13(3):485–494; doi: 10.1007/ s13534-023-00280-0
15. Polygerinos P, Galloway KC, Savage E, et al. Soft robotic glove for hand rehabilitation and task specific training. In: 2015 IEEE International Conference on Robotics and Automation (ICRA) IEEE: Seattle, WA, USA; 2015; pp. 2913–2919; doi: 10.1109/ICRA.2015.7139597
16. Wang Y, Kokubu S, Zhou Z, et al. Designing soft pneumatic actuators for thumb movements. IEEE Robot Autom Lett 2021;6(4):8450–8457; doi: 10.1109/LRA.2021.3105799
17. Ma K, Jiang Z, Gao S, et al. Design and analysis of fiber-reinforced soft actuators for wearable hand rehabilitation device. IEEE Robot Autom Lett 2022;7(3):6115–6122; doi: 10.1109/LRA.2022.3167063
18. Liu H, Wu C, Lin S, et al. From skin movement to wearable robotics: The case of robotic gloves. Soft Robot 2024;11(5): 755–766; doi: 10.1089/soro.2023.0115soro.2023.0115;
19. Cappello L, Galloway KC, Sanan S, et al. Exploiting textile mechanical anisotropy for fabric-based pneumatic actuators. Soft Robot 2018;5(5):662–674; doi: 10.1089/soro.2017.0076
20. Cappello L, Meyer JT, Galloway KC, et al. Assisting hand function after spinal cord injury with a fabric-based soft robotic glove. J Neuroeng Rehabil 2018;15(1):59; doi: 10 .1186/s12984-018-0391-x
21. Proietti T, Nuckols K, Grupper J, et al. Combining soft robotics and telerehabilitation for improving motor function after stroke. Wearable Technol 2024;5:e1; doi: 10.1017/wtc .2023.26

22. Ge L, Chen F, Wang D, et al. Design, modeling, and evaluation of fabric-based pneumatic actuators for soft wearable assistive gloves. Soft Robot 2020;7(5):583–596; doi: 10.1089/soro.2019.0105
23. Feng M, Yang D, Gu G. High-force fabric-based pneumatic actuators with asymmetric chambers and interference-reinforced structure for soft wearable assistive gloves. IEEE Robot Autom Lett 2021;6(2):3105–3111; doi: 10.1109/LRA.2021.3062588
24. Correia C, Nuckols K, Wagner D, et al. Improving grasp function after spinal cord injury with a soft robotic glove. IEEE Trans Neural Syst Rehabil Eng 2020;28(6):1407–1415.
25. Suulker C, Skach S, Althoefer K. Soft robotic fabric actuator with elastic bands for high force and bending performance in hand exoskeletons. IEEE Robot Autom Lett 2022;7(4):10621–10627; doi: 10.1109/LRA.2022.3194883
26. Jones LA, Lederman SJ. Human Hand Function. Oxford University Press; 2007.
27. Napier JR. STUDIES OF THE HANDS OF LIVING PRIMATES. Proc Zool Soc Lond 1960;134(4):647–657; doi: 10.1111/j.1469-7998.1960.tb05606.x
28. Landsmeer JMF. Power grip and precision handling. Ann Rheum Dis 1962;21(2):164–170; doi: 10.1136/ard.21.2.164
29. Sasaki D, Noritsugu T, Takaiwa M, et al. Wearable power assist device for hand grasping using pneumatic artificial rubber muscle. In: RO-MAN 2004. 13th IEEE International Workshop on Robot and Human Interactive Communication (IEEE Catalog No.04TH8759) IEEE: Kurashiki, Okayama, Japan; 2004; pp. 655–660; doi: 10.1109/ROMAN.2004.1374840
30. Li M, Zhuo Y, He B, et al. A 3D-printed soft hand exoskeleton with finger abduction assistance. In: 2019 16th International Conference on Ubiquitous Robots (UR) IEEE: Jeju, Korea (South); 2019; pp. 319–322; doi: 10.1109/URAI.2019.8768611
31. Yap HK, Khin PM, Koh TH, et al. A fully fabric-based bidirectional soft robotic glove for assistance and rehabilitation of hand impaired patients. IEEE Robot Autom Lett 2017;2(3):1383–1390; doi: 10.1109/LRA.2017.2669366
32. Yap H, Sebastian F, Wiedeman C, et al. Design and characterization of low-cost fabric-based flat pneumatic actuators for soft assistive glove application. IEEE Int Conf Rehabil Robot 2017;2017:1465–1470; doi: 10.1109/ICORR.2017.8009454In:
33. Lim DY-L, Lai H-S, Yeow RC-H. A bidirectional fabric-based soft robotic glove for hand function assistance in patients with chronic stroke. J Neuroeng Rehabil 2023;20(1):120; doi: 10.1186/s12984-023-01250-4
34. Wang Y, Kokubu S, Huang S, et al. Towards an extensive thumb assist: A comparison between whole-finger and modular types of soft pneumatic actuators. Appl Sci 2022;12(8):3735; doi: 10.3390/app12083735
35. Shiota K, Kokubu S, Tarvainen TVJ, et al. Enhanced Kapandji test evaluation of a soft robotic thumb rehabilitation device by developing a fiber-reinforced elastomer-actuator based 5-digit assist system. Robot Auton Syst 2019;111:20–30; doi: 10.1016/j.robot.2018.09.007
36. Feng M, Sun J, Yang D, et al. Characterization and modeling of fabric-based pneumatic actuators with asymmetric chambers for soft gloves. IEEE Robot Autom Lett 2024;9(11):10589–10596.
37. Feng M, Yang D, Ren L, et al. X-crossing pneumatic artificial muscles. Sci Adv 2023;9(38):eadi7133; doi: 10.1126/sciadv.adi7133
38. Feng M, Yang D, Sun J, et al. A pilot study on fabric-based pneumatic soft gloves for assisting patients with severe brachial plexus injury. IEEE Trans Biomed Eng 2025;72(11):3174–3185; doi: 10.1109/TBME.2025.3563348
39. Liu M-J, Xiong C-H, Hu D. Assessing the manipulative potentials of monkeys, apes and humans from hand proportions: Implications for hand evolution. n.d.
40. Boyer DM, Yapuncich GS, Chester SGB, et al. Hands of early primates. Am J Phys Anthropol 2013;152 (Suppl 57):33–78; doi: 10.1002/ajpa.22392
41. Schuenke M, Schulte E, Schumacher U, et al. General Anatomy and Musculoskeletal System (THIEME Atlas of Anatomy). 2010.
42. Denavit J, Hartenberg RS. A kinematic notation for lower-pair mechanisms based on matrices. J Appl Mech 1955;22(2):215–221; doi: 10.1115/1.4011045
43. Rose MD. Kinematics of the trapezium-1st metacarpal joint in extant anthropoids and Miocene hominoids. J Hum Evol 1992;22(4–5):255–266; doi: 10.1016/0047-2484(92)90058-H
44. Surgeons AA of O. Joint Motion: Method of Measuring and Recording. Churchill Livingstone; 1965.
45. Cotugno G, Althoefer K, Nanayakkara T. The role of the thumb: Study of finger motion in grasping and reachability space in human and robotic hands. IEEE Trans Syst Man Cybern, Syst 2017;47(7):1061–1070; doi: 10.1109/TSMC.2016.2531679
46. Kuo L-C, Chiu H-Y, Chang C-W, et al. Functional workspace for precision manipulation between thumb and fingers in normal hands. J Electromyogr Kinesiol 2009;19(5):829–839; doi: 10.1016/j.jelekin.2008.07.008
47. Lyle RC. A performance test for assessment of upper limb function in physical rehabilitation treatment and research. Int J Rehabil Res 1981;4(4):483–492; doi: 10.1097/00004356-198112000-00001
48. Yang Y, Fermuller C, Li Y, et al. Grasp type revisited: A modern perspective on a classical feature for vision. In: 2015 IEEE Conference on Computer Vision and Pattern Recognition (CVPR) IEEE: Boston, MA, USA; 2015; pp. 400–408; doi: 10.1109/CVPR.2015.7298637

Address correspondence to:
Guoying Gu
School of Mechanical Engineering
Shanghai Jiao Tong University
800 Dong Chuan Road
Shanghai 200240
China

E-mail: guguoying@sjtu.edu.cn